Nascent versus "Steady-State" Rovibrational Distributions in the Products of the $O(^3P) + O_3(\tilde{X}^1A)$ Reaction

P. J. S. B. Caridade, J. L. Llanio-Trujillo, and A. J. C. Varandas*

Departamento de Química, Universidade de Coimbra, 3004-535 Coimbra, Portugal

Received: June 13, 2003; In Final Form: October 6, 2003

We report a trajectory simulation study of the $O_2(v',j') + O_2(v'',j'')$ collisional process at a translational temperature of 1500 K with a view to compare the initial and final rovibrational distributions of the colliding species. As initial rotational and vibrational micropopulations we assume those calculated for the products of the forward title reaction. Rotational relaxation is found to occur to a larger extent than vibrational relaxation, a result that is in general agreement with experimental measurements for small and moderate delay times after the reaction $O + O_3 \rightarrow O_2(v',j') + O_2(v'',j'')$ has occurred. Rather than a single rotational temperature reported from the experiments, the simulations predict two disparate rotational temperatures close to those characterizing the nascent micropopulation. An increase in temperature due to vibrational−translational and rotational−translational relaxation processes is also predicted.

1. Introduction

A reaction of paramount importance in the upper atmosphere since Chapman's[1] proposal of the O_x catalytic cycle for ozone depletion is

$$O(^3P) + O_3(^1A_1) \rightarrow 2O_2(X^3\Sigma_g^-) \qquad (1)$$

Thus, it has been extensively studied both experimentally[2−6] and theoretically,[7−12] being known from experiments[6] specially designed for sensitive detection of O_2 excited states to be the dominant reaction when the reactants are in their ground electronic states; for a review on this and other four-atom reactions, including their reverse counterparts, with relevance in atmospheric chemistry, see ref 13.

Despite the importance of the title reaction, recent experimental work[6] has emphasized that its theoretical understanding may still be far from satisfactory. By photolizing ozone to produce $O(^3P)$, Mack et al.[6] observed the formation of vibrationally excited molecular oxygen in its ground electronic state, $O_2(v)$, via reaction 1. They also noted that the one-photon photolysis of ozone carried out at 532 nm cannot produce O_2 in $v \geq 10$, and that vibrational states above $v = 4$ were actually never observed. Thus, by choosing an appropriate pressure and delay time [note that the ozone photolysis is found[6] to be more than 10 times faster than reaction 1], both the nascent vibrational and rotational distributions could be probed. Of particular relevance from their study[6] is the suggestion that both O_2 molecules most likely emerge from the reaction with similar amounts of internal energy, which implies the simultaneous production of two vibrationally excited O_2 molecules. However, such a result is inconsistent with those obtained from dynamics calculations[6−8] that favor a spectator bond mechanism: one of the O_2 molecules is produced vibrationally excited ("hot") while the other is produced essentially in $v = 0$ ("cold"). This feature, which was first observed in dynamics studies[7] of the title reaction, has in fact been more recently confirmed[12] at the ab initio level via accurate complete-active-space self-consistent-field [commonly indicated as CASSCF(m,n) or CAS(m,n), where m stands for the number of active electrons and n the number of active orbitals in the full configuration interaction treatment of the molecular wave function; see, e.g., ref 14 and references therein] calculations of the minimum energy path for reaction.

A critical issue in a dynamics study is obviously the intrincacy and accuracy of the underlying potential energy surface(s) on which the reaction occurs. For the $O(^3P) + O_3(^1A) \rightarrow 2O_2(X^3\Sigma_g^-)$ reaction, the Wigner−Witmer rules suggest that the relevant potential energy surface corresponds to the lowest triplet state since it correlates with both reactants and products in their ground electronic states, although the backward reaction may evolve on singlet, triplet, and quintet surfaces. Since our analysis is based on the assumption of electronic adiabaticity, we will focus on the lowest triplet surface of O_4 (for possible nonadiabatic effects, see ref 15 and references therein).

For tetraoxygen in its ground triplet state, the task of calculating by ab initio methods the corresponding potential energy surface with chemical accuracy (1 kcal mol^{-1}) is overwhelming. Such a difficulty gets compounded by the fact that the calculations and modeling must cover the six-dimensional (6D) configurational space of the supermolecule. By following Hernández-Lamoneda and Ramírez-Solis,[16,17] we have recently[18] calculated by accurate ab initio methods the properties of the transition state for the title reaction, including the force field that was unknown thus far. Moreover, we have used such data to obtain an improved double many-body expansion[19−21] potential energy surface (DMBE II) for ground-triplet O_4. Thus, DMBE II mimics the best available ab initio estimate of the force field at the saddle point for reaction 1 while its barrier height has been constrained to have a value identical with that in DMBE I,[7] since this is supported by the thermal rate coefficient data[2−5,22] (for other specific details, see section 2). Ignoring aspects related to possible conical intersections which are known[23] to appear in the $O_3(^1A_1)$ fragment and most likely extend to other regions of the O_4 potential energy surface, the DMBE II surface should therefore describe reliably the dynamics of reaction 1. In fact, a dynamics and kinetics study of the title reaction employing the quasiclassical trajectory (QCT) method and the DMBE II surface has given[12] thermal rate coefficients in very good agreement with experiment over

* Address correspondence to this author. E-mail: varandas@qtvs1.qui.uc.pt.

10.1021/jp030756v CCC: $25.00
Published on Web 11/22/2003

the whole range of temperatures where the calculations and experimental data overlap. We emphasize though that, as in previous studies with DMBE I,[7] the QCT results predict that only one of the O_2 bonds emerges vibrationally excited with the remainder of the exothermicity channeled into rotation and translation of the two O_2 molecules. Thus, no breakdown of the spectator bond mechanism is observed. Although this result may bring to question the reliability of both DMBE I and DMBE II potential energy surfaces employed for the dynamics calculations, we emphasize that a detailed structural analysis[12] of the minimum energy path for reaction using CAS(16,12) calculations has corroborated such a prediction. Of course, one may still argue that the specific mechanism of the reaction is a dynamical property that cannot be "confirmed" by an electronic structure calculation. To go further, one requires the inclusion of possible nonadiabatic effects and accurate quantum dynamics calculations on the relevant electronic manifold, an issue that is outside the scope of the present work.

In ref 12, we have also advanced a tentative explanation for the existing theoretical versus experimental dispute concerning the rotational distribution of the vibrationally hot O_2 molecules in the products. We conjectured that the observed rotational temperature could be partly due to a prompt rotational quenching after reaction. From their experimental work, Mack et al.[6] observed that, under pressure−time conditions of $p\tau = 1 \times 10^{-6}$ Torr s, rotational relaxation is in general substantial but vibrational relaxation is unimportant. Note that reaction 1 occurs much faster than the vibrational and rotational relaxation processes, being essentially complete at their start. Quoting the authors:[6] "relative intensities taken at a value of $p\tau = 1 \times 10^{-6}$ Torr s were found to be rotationally relaxed, but immune from vibrational relaxation". Since typical pressures in the experiments were 1−2 Torr, and hence are comparable to those observed in the middle atmosphere, it follows that vibrational and rotational relaxation processes should be rather slow on the temporal scale of reaction 1. It is therefore unlikely that more than a few collisions occur before reaction takes place, which supports the scheme recently suggested by one of us[24] to obtain "steady-state" distributions. This is based on the assumption that the distribution after an ensemble of single-collisions mimics the overall result from relaxation (in the sense of de-excitation, but to a smaller extent also excitation) in multiple collision processes especially having in mind that new $O_2(v)$ molecules are meanwhile formed via reaction 1. Of course, the plausibility of such an assumption can only be tested by a computational simulation of all involved processes.

In the experiments performed by Mack et al.,[6] the best rotational distributions were observed for several vibrational states, with the highest quality data being obtained for $O_2(v = 12-14)$ at the smallest value of $p\tau$ ($=8 \times 10^{-8}$ to 1.2×10^{-7} Torr s). In this case, a plot of the logarithm of the peak heights divided by $2j + 1$ shows a straight-line shape, suggesting that an effective rotational temperature could still be defined. Thus, a significant amount of rotational relaxation may occur even under such experimental conditions. It turns out that the estimated rotational temperature (1400 ± 300 K) is relatively small when compared to the highest of the two rotational temperatures that we have estimated by running classical trajectories.[18] Such calculations suggested that the set of vibrationally hot O_2 molecules may be divided in two subsets: one (S1) characterized by high-rotational states and an effective rotational temperature of $T_{rot}^{hot}(\text{high } j) = 27000$ K; the other (S2) consisting of rotationally cold $O_2(v)$ with an effective temperature of $T_{rot}^{hot}(\text{low } j) = 1267$ K. In view of the experimental results, this led us to conjecture that rotational relaxation may take place soon after reaction occurs. However, a second thought suggests that the disparity of temperatures involved may prevent S1 and S2 from exchanging energy via a rotational−rotational (RR) energy transfer mechanism, while the possibility of vibrational−rotational (VR) energy exchange remains viable. Of course, experimental measurements at very short delay times could settle the issue of characterizing the nascent micropopulations, but such measurements were taken[6] in time only down to 60 ns and hence cannot give a definite answer to the above query. Strictly speaking, the measured distributions may not be the nascent ones but those actually present in the reaction vessel for a pre-specified delay time, which for the present purposes will be modeled by the "steady-state" distributions[24] mentioned above. Computer inelastic scattering simulations similar to those reported elsewhere[24] could therefore be valuable to clarify the situation. The question is then of what happens, upon collisions with the surrounding molecules, to the nascent $O_2(v)$ distributions of reaction 1 shortly after being produced. In other words: How different are the nascent and "steady-state" distributions at a given temperature? Because one expects relaxation to be enhanced with increasing temperature, we will consider a temperature of 1500 K in the present work.

An answer to the above issues will be attempted by running quasiclassical trajectories[13,25,26] on the recent DMBE II $O_4(^3A)$ potential energy surface. Such a methodology can be justified a priori from the large atomic masses involved, and a posteriori by the excellent agreement between the QCT calculations[7,8] and approximate quantum-dynamics results[9,10] with use of the same (DMBE I) potential energy surface. The paper is organized as follows: Section 2 provides a brief description of the $O_4(^3A)$ DMBE II potential energy surface, while the trajectory calculations are reported in section 3, and discussed in section 4. The conclusions are given in section 5.

2. Potential Energy Surface

All calculations reported in the present work employ the DMBE II potential energy surface for ground-triplet O_4. Since it has been discussed in detail elsewhere,[12,18] we refer only to the basic features that may be relevant for the present analysis. It was obtained by adding an extra four-body extended Hartree−Fock energy term to DMBE I, with the coefficients calibrated via a nonlinear least-squares fit such as to reproduce the geometry (which coincides with that reported by Hernández-Lamoneda and Ramírez-Solis[17]) and (approximately) the quadratic force constants[18] obtained from CAS(16,12) calculations employing a [6-311G] Pople-type basis set[27] with polarization functions for a high level of correlation.[28] Special care has been taken to model the barrier height of reaction 1. In fact, since the ab initio CAS(16,12) calculations predicted it to be 8 kcal mol^{-1} higher than the activation energy recommended by the IUPAC Subcommittee on Gas Kinetics Data Evaluation for Atmospheric Chemistry,[22] such a limitation was overcome by constraining the barrier height to be 3.4 kcal mol^{-1} (i.e., the barrier height in DMBE I) while its location was set at the geometry predicted by the ab initio calculations. Unfortunately, after publication of DMBE II, a detailed search of its stationary points has shown a spurious deep minimum for D_{2d} geometries. However, a high energy seam separates the spurious D_{2d} minimum from the $O_2 + O_2$ asymptote, and hence it should have no implications in classical dynamics studies for most collision energies of practical relevance. In fact, test studies of reaction 1 and the nonreactive $O_2 + O_2$ collisional process show that no drastic differences occur between the results obtained with DMBE I and DMBE II. Figure 1 illustrates the DMBE II

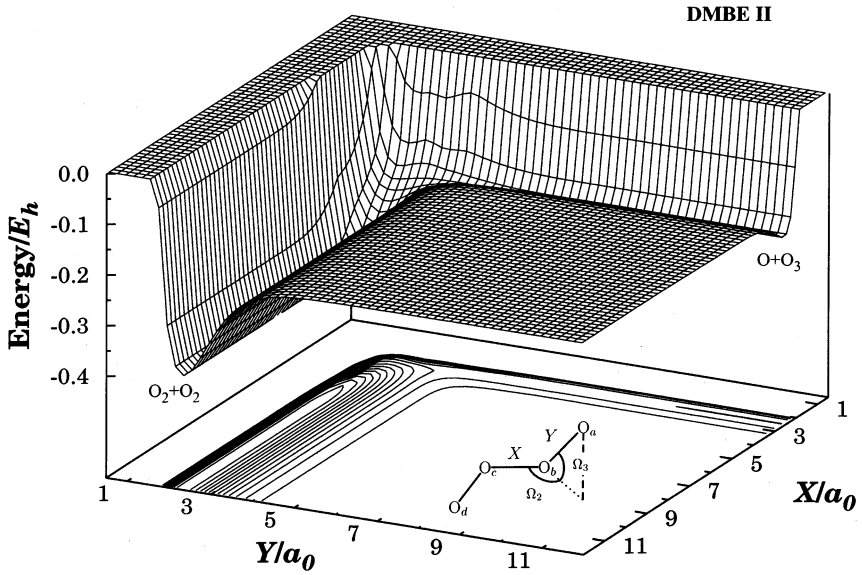

Figure 1. A perspective view of the DMBE II potential energy surfaces for the lowest triplet state of O_4. See also the text.

potential energy surface for the attack of an oxygen atom on the terminal atom of ozone. Note that *X* represents the distance between the two middle atoms (*b* and *c*), while *Y* is the distance between atoms *a* and *b*. Note further that the energy has been minimized at each (*X*,*Y*) geometry by optimizing the polar angles Ω_2 and Ω_3, keeping the O_cO_d bond distance and the angle $\angle O_bO_cO_d$ constrained at their equilibrium values in ozone. The differences between DMBE II and DMBE I are very subtle, and invisible to the naked eye for the covered regions of configuration space.

3. Trajectory Calculations

To run the quasiclassical trajectories, we have utilized the MERCURY/VENUS96[29] codes, which have been suitably modified to (a) accommodate the DMBE II[18] potential energy surface for ground-triplet tetraoxygen, (b) recognize the various reaction channels,[30] and (c) use several rovibrational distributions (which are exact for the diatomic curves employed in constructing the DMBE potential energy surfaces). To compare the nascent and "steady-state" distributions, we have considered as initial conditions for the colliding diatomics those of the products of reaction 1 as if the clock was started at the end of the trajectories for the forward reaction.[12] Of course, the calculated nascent distributions differ to some extent from those experimentally reported,[6] but this is not expected to alter drastically the major conclusions. For brevity, we will denote by the subscript "nasc" the initial (nascent) distribution while we use "ss" for the (final, nonequilibrium) steady-state distribution.

The procedure then involved the following steps.[24] First, we define the initial states of the colliding species in the $O_2(v',j') + O_2(v'',j'')$ inelastic process. The initial vibrational distribution of the vibrationally hot molecules, hereafter represented by $O_2(v')$, has been chosen to mimic the distribution reported elsewhere,[12] which is well described by the form

$$P_{v'}^{\text{hot}} = B \exp[-b(v' - v'_0)^2] \tag{2}$$

where the optimum values are $B = 0.33$, $b = 0.0698$, and $v'_0 = 10.5$. The simulated distribution is shown by the dashed line in panels a of Figures 2 and 3, while the target initial distribution function in eq 2 is indicated by a dash−dot line. Note that all curves have been normalized at the absolute maximum of the target function (the same applies to the other micropopulations that will be described next), which explains the fact that some probabilities in the final distribution may attain values >1.0. Of course, such values have no other meaning except that of offering a direct comparison with the initial micropopulations. In turn, the corresponding rotational distribution has been fitted to the form

$$P_{j'}^{\text{hot}} = \sum_{m=1}^{2} A_m \exp[-a_m(j' - j'_m)^2] \tag{3}$$

where $A_1 = 0.30$, $A_2 = 0.62$, $a_1 = 0.00391$, $a_2 = 0.00454$, $j'_1 = 46$, and $j'_2 = 74$. This is shown in panels b of Figures 2 and 3, where a type of line convention similar to that used for the vibrational distribution is employed. It should be recalled at this point that only odd rotational states are allowed for O_2. No attempt has therefore been made to distinguish the S1 and S2 subsets of rotationally excited $O_2(v)$ molecules.

Two possible variants can now be considered for the rovibrational distributions in the set of $O_2(v'')$ colliding partners. In case I, we assume that $O_2(v'')$ are the vibrationally cold molecules formed in reaction 1, being the vibrational micropopulation modeled by

$$P_{v''}^{\text{cold}} = \exp(-cv'') \tag{4}$$

where $c = 1.94$. In turn, the corresponding rotational contribution has been represented by a single Gaussian in eq 3, with the parameters obtained by fitting the results of ref 12: $A_1 = 1.0$, $a_1 = 0.00384$, and $j'_1 = 33$. The initial vibrational and rotational distributions so obtained are illustrated in panels c and d of Figure 2, respectively. Although the target vibrational function and the actual discretized distribution seem to differ significantly, this is an artifact of the representation due to the small number of bins that are populated. Case II assumes that $O_2(v'')$ includes both the vibrationally hot and cold molecules, being denoted for brevity as "total". The corresponding vibrational and rotational distributions are in this case defined by the following bimodal distributions:

$$P_{v''}^{\text{total}} = P_{v'}^{\text{hot}} + P_{v''}^{\text{cold}} \tag{5}$$

$$P_{j''}^{\text{total}} = P_{j'}^{\text{hot}} + P_{j''}^{\text{cold}} \tag{6}$$

which are depicted in panels c and d of Figure 3.

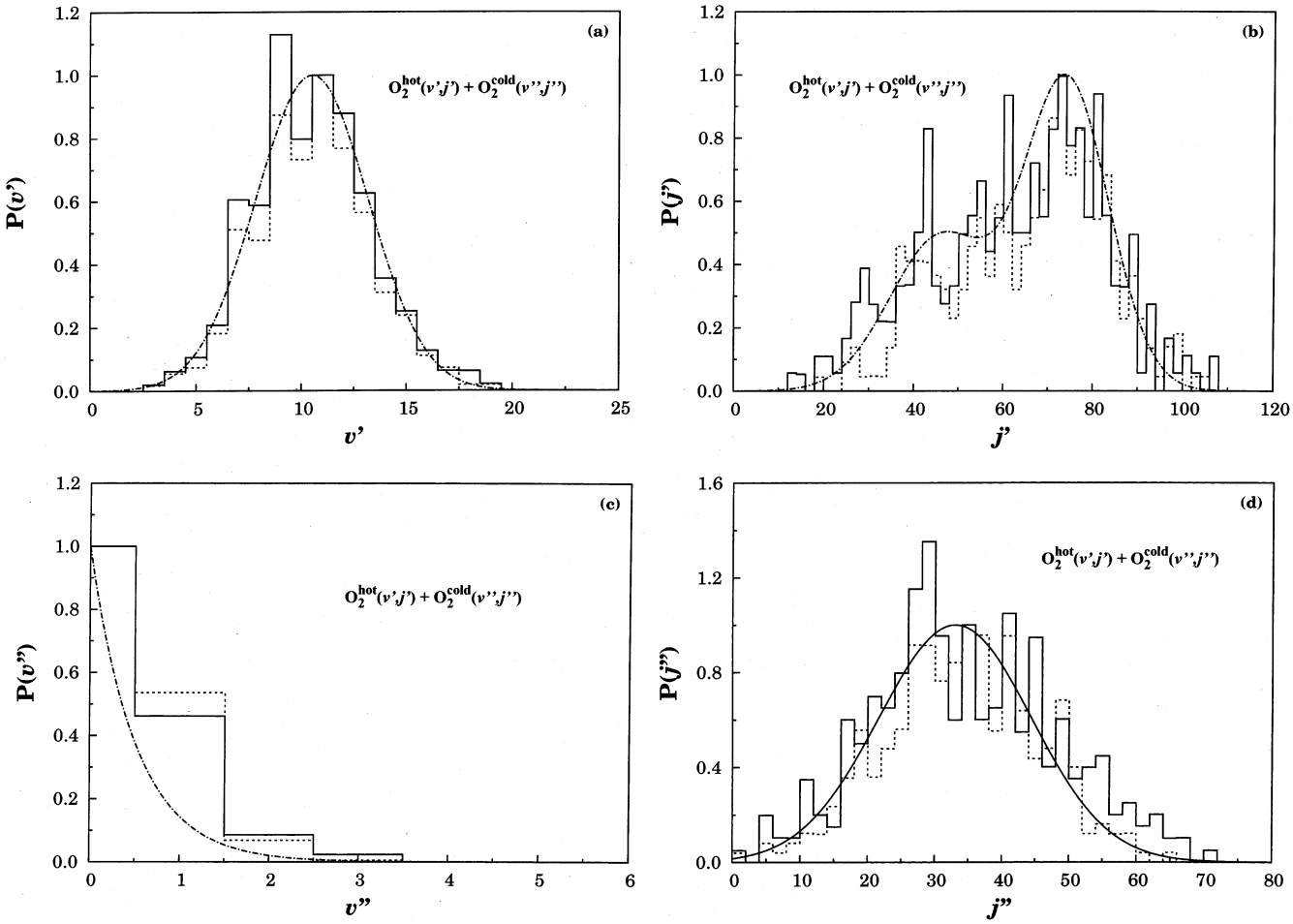

Figure 2. Vibrational and rotational distributions in the simulation study of the vibrationally hot−vibrationally cold inelastic collisional processes: (a and b) hot oxygen molecules; (c and d) cold oxygen molecules. The translational energy is thermalized at $T = 1500$ K. Key: - · -, target (initial) distribution; - - -, initial distribution (actual sampling); —, final distribution. See also the text.

A computer simulation employing the traditional approach (ref 31 and references therein) has shown that the above vibrational and rotational distributions can be accurately mimicked with a few thousand trajectories, and it is the very conservative results obtained in this way by using a total of 10^4 trajectories that we consider as the initial distributions. With use of such micropopulations, the values of v and j for every trajectory can be sampled by the procedure used in ref 24. All other initial conditions are set according to the standard trajectory procedure. Thus, for the two cases (hot−cold and hot−"total") defined above, the maximum value of the impact parameter (b_{max}) has been chosen as the largest value obtained for the O + O_3 reaction,[12] i.e., $b_{max} = 3.1$ Å. In turn, the initial distance between the reactants has been fixed at 9 Å such as to give a negligible interaction between the two reactant oxygen molecules. Moreover, the translational energy has been sampled by assuming a Maxwell−Boltzmann distribution for a typical temperature of $T = 1500$ K. Note that such a temperature is similar to the measured average rotational temperature of the "steady-state" distribution when the delay time is 60 ns.[6]

After integration of Hamilton's equations, the rotational quantum number has been determined from the classical orbital angular momentum, L, of each molecule

$$L^2 = j(j+1)\hbar^2 \tag{7}$$

For the calculation of the vibrational quantum number we have adopted the usual semiclassical quantization scheme.[29] Although in previous work we have used the more traditional boxing procedure (see ref 24), the comparison of these two methods gives the same result within the error margins. Note that a major advantage of the semiclassical procedure is to avoid a decomposition of the internal energy into vibrational and rotational components (see ref 12 for a critical assessment).

For a given temperature, the rate constant of the collisional process $O_2(v_i', j_i') + O_2(v_i'', j_i'') \rightarrow O_2(v_f', j_f') + O_2(v_f'', j_f'')$, denoted by x, is given by the usual expression

$$k_x(T) = g_e\left(\frac{8k_BT}{\pi\mu}\right)^{1/2}\sigma_x(T) \tag{8}$$

where k_B is the Boltzmann constant, μ the reduced mass of the reactants, $g_e = {}^1/_3$ is the electronic degeneracy, and $\sigma_x(T) = \pi b_{max}^2 N_x/N$ is the cross section (N_x denotes the number of trajectories leading to the x process out of a total of N trajectories); the statistical 68% confidence interval is $\Delta k_x(T) = k_x(T)(N - N_x/NN_x)^{1/2}$.

4. Results and Discussion

Figures 2 and 3 compare the initial and final distributions for the two simulation experiments considered in the present work. Specifically, Figure 2 shows the outcome distributions for collisions involving vibrationally hot O_2 molecules with cold ones (case I), while Figure 3 shows similar results but for collisions of vibrationally hot O_2 molecules with the total vibrational micropopulation (case II). The notable feature from the vibrational distributions is the striking similarity between

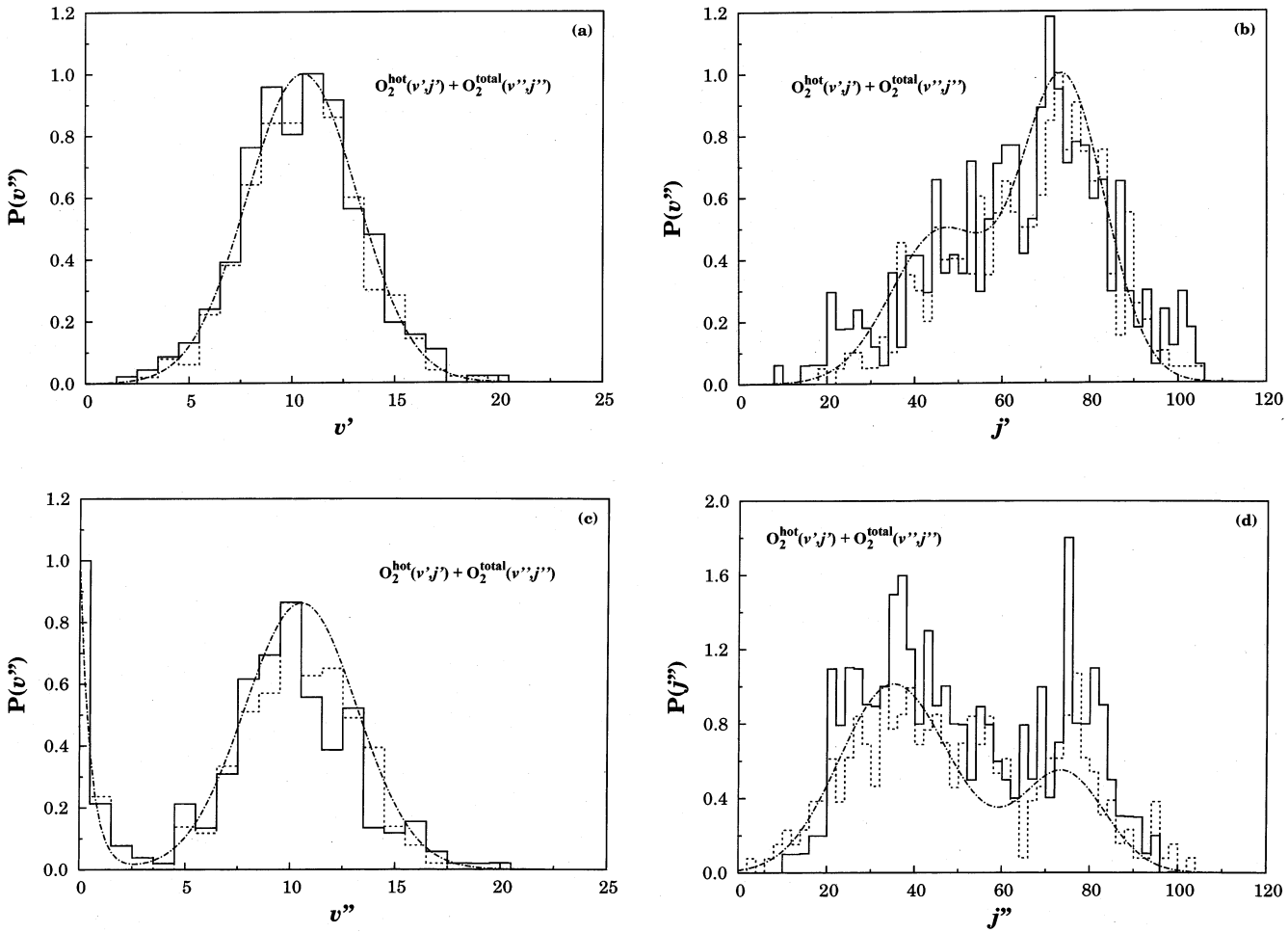

Figure 3. As in Figure 2 but for the vibrational hot−'total' collisional process: (a and b) hot oxygen molecules; (c and d) "total". Key: - • -, target (initial) distribution; - - -, initial distribution (actual sampling); —, final distribution.

their initial and final shapes, with a smaller degree of similarity applying to the rotational distributions. This implies that the vibrational "steady-state" distributions do not differ drastically from the nascent ones, especially in case II. Although the initial micropopulations may not coincide with the experimental observation of Mack et al.,[6] such results may be viewed as supporting their findings that vibrational relaxation is unimportant, although rotational relaxation could be substantial. It also agrees with a recent observation by one of us[24] that under the conditions found in the middle atmosphere, vibrational relaxation is expected to be less significant than is usually believed. It should also be recalled our difficulty[12] in assigning a rotational temperature, even when reaction 1 has started from thermalized reactants. This led to a tentative assignment of two coexisting types of $O_2(v)$ molecules having distinct rotational temperatures, namely for $v = 12$. The present results show that the rotational thermalization remains incomplete even when the two rotational ensembles are allowed to interact with each other. We should note that a choice of a different bining size does not improve the lack of statistics due to the limited number of trajectories run. Moreover, doubling its size may have the misleading effect of centering the bins at even rotational numbers, which are forbidden for O_2. In summary, one expects that the temperatures in the steady state for $v = 12$ do not differ significantly from those reported elsewhere[12] ($T = 1267$ and 27000 K for the vibrationally cold and hot O_2 molecules, respectively).

Despite the fact that the initial and final distributions show similar patterns, this by no means implies that there has not been a significant energy transfer at the microscopic level. A quantitative assessment is presented in Tables 1 and 2. In general, deactivation is more pronounced that activation in both cases I and II. For case I, the number of vibrationally hot molecules that cooled is 1484 (14.8%), while in case II the number increased to 2343 (23.4%). Conversely, the corresponding numbers for vibrational warming are 1065 (9%) in case I and 1905 (11%) in case II. Other relevant indicators are the averaged vibrational and rotational quantum numbers before and after collision. For case I, the average vibrational quantum number in the nascent distribution is $\langle v' \rangle_{nasc} = 10.53$ while the corresponding number in the "steady-state" distribution is $\langle v' \rangle_{ss} = 9.93$. Note from Figure 4 that transitions (no attempt has been made to discriminate activation and deactivation processes) involving as much as 4 vibrational quanta have been observed for the hot molecules in hot−cold collisions while in the hot−"total" case this number reached 6 vibrational quanta. However, the predicted law for multiquantum vibrational transitions ($1 \leq \Delta v \leq 4$ or $1 \leq \Delta v \leq 6$) is found to vary approximately as an inverse exponential of the number of multiquanta involved, which implies a low probability of occurrence for high multiquanta transitions. Such a result agrees with recent measurements on $O_2 + O_2$ collisions with oxygen molecules prepared in vibrational levels between $v = 23$ and $v = 27$, where multiquantum transitions involving 8 or 9 vibrational quanta have been observed.[32] Note that such high quanta vibrational

TABLE 1. A Summary of the Major Energy Transfer Processes for the Hot−Cold $O_2 + O_2$ Collisional Events

type	process[a] ($\equiv x$)	N_x	P_x, %	k_x, 10^{-13} cm^3 s^{-1}
deactivation				
VV	$(v'_i, j'_i) + (v''_i, j''_i) \rightarrow (v'_i - 1, j'_f) + (v''_i + 1, j''_f)$	241	2.4	34.2 ± 2.2
VV	$(v'_i, j'_i) + (v''_i, j''_i) \rightarrow (v'_i - 2, j'_f) + (v''_i + 2, j''_f)$	n.o.		
VR	$(v'_i, j'_i) + (v''_i, j''_i) \rightarrow (v'_i - 1, j'_f) + (v''_i, j''_f)$	849	8.5	120.4 ± 4.0
VR	$(v'_i, j'_i) + (v''_i, j''_i) \rightarrow (v'_i - 2, j'_f) + (v''_i, j''_f)$	184	1.8	26.1 ± 1.9
VR	$(v'_i, j'_i) + (v''_i, j''_i) \rightarrow (v'_i - n, j'_f) + (v''_i, j''_f)$	60	0.6	8.5 ± 1.1
RT	$(v'_i, j'_i) + (v''_i, j''_i) \rightarrow (v'_i, j'_f < j'_i) + (v''_i, j''_f < j''_i)$	1062	10.6	150.6 ± 4.4
RR	$(v'_i, j'_i) + (v''_i, j''_i) \rightarrow (v'_i, j'_f < j_i) + (v''_i, j''_f)$	3419	34.2	484.8 ± 6.7
activation				
VV	$(v'_i, j'_i) + (v''_i, j''_i) \rightarrow (v'_i + 1, j'_f) + (v''_i - 1, j''_f)$	122	1.2	17.3 ± 1.6
VV	$(v'_i, j'_i) + (v''_i, j''_i) \rightarrow (v'_i + 2, j'_f) + (v''_i - 2, j''_f)$	n.o.		
VR	$(v'_i, j'_i) + (v''_i, j''_i) \rightarrow (v'_i + 1, j'_f) + (v''_i, j''_f)$	698	7.0	99.0 ± 3.6
VR	$(v'_i, j'_i) + (v''_i, j''_i) \rightarrow (v'_i + 2, j'_f) + (v''_i, j''_f)$	91	0.9	12.9 ± 1.3
VR	$(v'_i, j'_i) + (v''_i, j''_i) \rightarrow (v'_i + n, j'_f) + (v''_i, j''_f)$	n.o.		
RT	$(v'_i, j'_i) + (v''_i, j''_i) \rightarrow (v'_i, j'_f > j'_i) + (v''_i, j''_f > j''_i)$	152	1.5	21.6 ± 1.7
RR	$(v'_i, j'_i) + (v''_i, j''_i) \rightarrow (v'_i, j'_f > j'_i) + (v''_i, j''_f)$	1548	15.5	219.5 ± 5.1

[a] The symbol n in the VR-type processes indicates the size of the vibrational quantum jump, when this is larger than 2.

TABLE 2. A Summary of the Major Energy Transfer Processes for the Hot-'total' $O_2 + O_2$ Collisional Events

type	process[a] ($\equiv x$)	N_x	P_x, %	k_x, 10^{-13} cm^3 s^{-1}
deactivation				
VV	$(v'_i, j'_i) + (v''_i, j''_i) \rightarrow (v'_i - 1, j'_f) + (v''_i + 1, j''_f)$	246	2.5	$34.2 \pm +2.2$
VV	$(v'_i, j'_i) + (v''_i, j''_i) \rightarrow (v'_i - 2, j'_f) + (v''_i + 2, j''_f)$	62	0.6	8.8 ± 1.1
VV	$(v'_i, j'_i) + (v''_i, j''_i) \rightarrow (v'_i - n, j'_f) + (v''_i + n, j''_f)$	n.o.	-	-
VR	$(v'_i, j'_i) + (v''_i, j''_i) \rightarrow (v'_i - 1, j'_f) + (v''_i, j''_f)$	499	5.0	70.8 ± 3.1
VR	$(v'_i, j'_i) + (v''_i, j''_i) \rightarrow (v'_i - 2, j'_f) + (v''_i, j''_f)$	31	0.3	4.4 ± 0.8
VR	$(v'_i, j'_i) + (v''_i, j''_i) \rightarrow (v'_i - n, j'_f) + (v''_i, j''_f)$	31	0.3	4.4 ± 0.8
RT	$(v'_i, j'_i) + (v''_i, j''_i) \rightarrow (v'_i, j'_f < j'_i) + (v''_i, j''_f < j''_i)$	342	3.4	48.5 ± 2.6
RR	$(v'_i, j'_i) + (v''_i, j''_i) \rightarrow (v'_i, j'_f < j'_i) + (v''_i, j''_f)$	1530	15.3	216.9 ± 5.1
activation				
VV	$(v'_i, j'_i) + (v''_i, j''_i) \rightarrow (v'_i + 1, j'_f) + (v''_i - 1, j''_f)$	407	4.1	57.7 ± 2.8
VV	$(v'_i, j'_i) + (v''_i, j''_i) \rightarrow (v'_i + 2, j'_f) + (v''_i - 2, j''_f)$	125	1.2	17.7 ± 1.6
VV	$(v'_i, j'_i) + (v''_i, j''_i) \rightarrow (v'_i + n, j'_f) + (v''_i - n, j''_f)$	n.o.	-	-
VR	$(v'_i, j'_i) + (v''_i, j''_i) \rightarrow (v'_i + 1, j'_f) + (v''_i, j''_f)$	470	4.7	66.6 ± 3.0
VR	$(v'_i, j'_i) + (v''_i, j''_i) \rightarrow (v'_i + 2, j'_f) + (v''_i, j''_f)$	62	0.6	8.8 ± 1.1
VR	$(v'_i, j'_i) + (v''_i, j''_i) \rightarrow (v'_i + n, j'_f) + (v''_i, j''_f)$	31	0.3	4.4 ± 0.8
RT	$(v'_i, j'_i) + (v''_i, j''_i) \rightarrow (v'_i, j'_f > j'_i) + (v''_i, j''_f > j''_i)$	158	1.6	22.4 ± 1.8
RR	$(v'_i, j'_i) + (v''_i, j''_i) \rightarrow (v'_i, j'_f > j'_i) + (v''_i, j''_f)$	1221	12.2	173.1 ± 4.6

[a] The symbol n in the VR-type processes indicates the size of the vibrational quantum jump, when this is larger than 2.

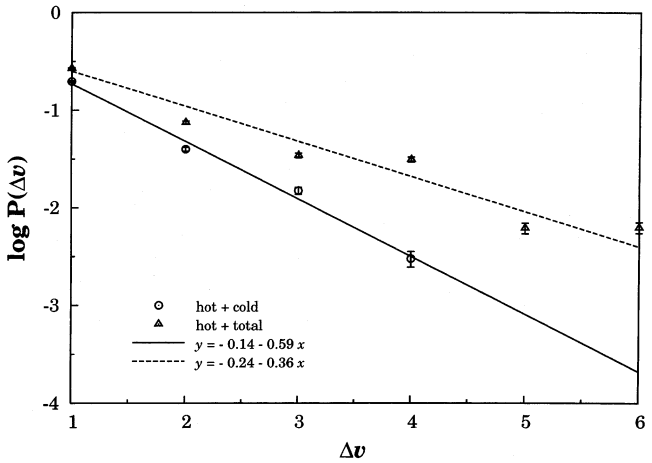

Figure 4. Probability of occurrence of multiquanta vibrational transitions in hot−cold and hot−"total" collisions. Also shown are the statistical error bars. See also the text.

transitions observed in the present work refer to VR (vibrational−rotational) and VT (vibrational−translational) processes, since for VV transitions the only observed cases were $\Delta v = 1$ or 2. This result seems to be in accord with the work of Balakrishnan et al.,[33] who noted that, for the highly vibrationally excited case $O_2(v' = 25) + O_2(v'' = 0)$, the VT process is the major quenching mechanism. We further note that transitions $|\Delta v| = \pm 1$ are expected to dominate for harmonic oscillators, although multiquantum jumps are included even in the traditional Landau−Teller model of vibrational energy transfer with use of an harmonic oscillator target.[34] Of course, multiquantum transitions may also occur for realistic anharmonic oscillators such as the O_2 diatomic curves used in the DMBE potential energy surface. Correspondingly, the results for the nascent and "steady-state" rotational distributions are $\langle j' \rangle_{nasc} = 65.58$ and $\langle j' \rangle_{ss} = 61.78$. This may in short be indicated as $\langle v' \rangle_{nasc \rightarrow ss} = 10.53 \rightarrow 9.93$ and $\langle j' \rangle_{nasc \rightarrow ss} = 65.58 \rightarrow 61.78$. Instead, the corresponding changes for the "bath" molecules are the following: $\langle v'' \rangle_{nasc \rightarrow ss} = 0.43 \rightarrow 0.00$ and $\langle j'' \rangle_{nasc \rightarrow ss} = 34.07 \rightarrow 33.95$. In turn, case II is characterized by $\langle v' \rangle_{nasc \rightarrow ss} = 10.45 \rightarrow 9.88$, $\langle j' \rangle_{nasc \rightarrow ss} = 65.15 \rightarrow 62.98$, $\langle v'' \rangle_{nasc \rightarrow ss} = 8.33 \rightarrow 7.63$, and $\langle j'' \rangle_{nasc \rightarrow ss} = 51.04 \rightarrow 50.45$. Interestingly, both the hot and "bath" molecules suffer on average a slight vibrational and rotational cooling. This implies that the internal energy of both species is transferred to a significant extent to the translational degrees of freedom. This leads us to predict a temperature increase of the gas inside the reaction vessel with delay time, which may be estimated from the excess kinetic (translational) energy in the bath after relaxation took place (i.e., in the "steady-state" distribution), $\Delta E_{tr}^{nasc \rightarrow ss}$, and the heat capacity of the gas. For case I, one has $\Delta E_{tr}^{nasc \rightarrow ss} = 0.75$ kcal mol^{-1}, which leads us to predict a temperature increase of $\Delta T = 149$ K, while in case II the result is $\Delta E_{tr}^{nasc \rightarrow ss} = 0.81$ kcal mol^{-1}, leading to a predicted temperature rise of $\Delta T = 161$ K. We note that Mack et al.[6] observed that vibrational relaxation was small, and that significant rotational relaxation occurred as a function of time, which may imply that the translational energy increased with time. However, such a conclusion is not obvious from their results and

certainly the extent of internal energy transferred to translational motion has not been quantified. Of course, a word of caution is necessary in comparing with experiment, since the micropopulation distributions used in the simulations are not identical with the measured ones.

Tables 1 and Table 2 summarize in more detail some of the most important energy transfer processes involved. Despite our remarks above, they have been catalogued according to their VV and VR characteristics, leaving aside the translational degrees of freedom. For example, a process labeled VR may also have a strong component of vibrational-to-translation energy transfer, which we have made no attempt to discriminate in this work. Perhaps the most significant result is the fact that the vibrational relaxation process $O_2(v_i', j_i') + O_2(v_i'', j_i'') \rightarrow O_2(v_i' - 1, j_f') + O_2(v_i'' + 1, j_f'')$ is the dominant one for deactivation in case II while $O_2(v_i', j_i') + O_2(v_i'', j_i'') \rightarrow O_2(v_i' - 1, j_f') + O_2(v'', j_f'')$ dominates in case I. This may be understood from the energy gap of the vibrational quanta involved in the transitions. Since in case II the gap between the initial vibrational states of the two colliding molecules is on average smaller than that for case I, one then expects one-quantum vibrational cooling of the hot molecules to be accompanied by one-quantum vibrational warming of the cold ones. Conversely, in case I, the vibrational gap between the two colliding partners is large, which leads one to expect vibrational cooling of the hot molecules to result mainly from VR and VT energy transfer processes.

From the above results, we may calculate the thermal rate coefficients by using eq 8, which are also shown in Tables 1 and 2. Of these, the result for the total VV energy transfer may be compared with the corresponding value obtained from Table 3 of ref 35 at $T = 1000$ K, using a potential energy surface that does not allow for reaction. One gets for the latter (suitably multiplied by g_e) the value of $\sum_{v'} k_{v',0\rightarrow v'-1,1} = 20 \times 10^{-13}$ cm^3 s^{-1}, which compares well with the result of $(34.2 \pm 2.2) \times 10^{-13}$ cm^3 s^{-1} reported in Tables 1 and 2 for $T = 1500$ K. Finally, we observe from these tables that one-quanta vibrational transitions predominate, which is a common result (ref 35 and references therein) for collisional partners involving long-range quadrupole−quadrupole electrostatic interactions.

5. Conclusions

To the extent that the simulation process[24] used in the present work offers a plausible scheme to describe relaxation in a dilute gas at vibrational and rotational termodynamic disequilibrium, our results suggest that rotational relaxation is in general more substantial than vibrational relaxation. This follows the general trend experimentally observed by Mack et al.[6] under pressure−time conditions of $p\tau = 1 \times 10^{-6}$ Torr s. Because some significant differences between experiment and theory remain to be settled, the problem calls for further work to be fully explained. Theoretically, a more accurate potential energy surface (or surfaces) may be required together with a full-dimensional quantum treatment of the underlying nuclear dynamics. Experimentally, the possibility of reevaluating the experimental results should also not be excluded. A final comment goes to the typical pressures observed in the experiments[6] (1−2 Torr), which are comparable to those observed in the middle atmosphere. Vibrational and rotational relaxation processes may therefore be expected to be rather slow in the temporal scale of the atmospheric reaction 1. As a result, it seems plausible to assume that no more than a few collisions occur under such conditions before reaction takes place, and hence *local thermodynamic disequilibrium* must be considered if accurate results are to be expected from atmospheric modeling studies in the middle atmosphere.[24,36,37]

Acknowledgment. This work has the support of Fundação para a Ciência e a Tecnologia, Portugal, via project POCTI/40154/QUI/2001 and FEDER.

References and Notes

(1) Chapman, S. *Mem. R. Metereol. Soc.* **1930**, *3*, 103.
(2) McCrumb, J. L.; Kaufman, F. *J. Chem. Phys.* **1972**, *57*, 1270.
(3) Davis, D. D.; Wong, W.; Lephardt, J. *Chem. Phys. Lett.* **1973**, *22*, 273.
(4) West, G. A.; Weston, R. E., Jr.; Flynn, G. W. *Chem. Phys. Lett.* **1978**, *56*, 429.
(5) Wine, P. H.; Nicovich, J. M.; Thompson, R. J.; Ravishankara, A. R. *J. Phys. Chem.* **1983**, *87*, 3948.
(6) Mack, J. A.; Huang, Y.; Wodtke, A. M.; Schatz, G. C. *J. Chem. Phys.* **1996**, *105*, 7495.
(7) Varandas, A. J. C.; Pais, A. A. C. C. *Theoretical and Computational Models for Organic Chemistry*; Formosinho, S., Czismadia, I., Arnaut, L., Eds.; Kluwer: Dordrecht, The Netherlands, 1991; p 55.
(8) Varandas, A. J. C.; Wang, W. *Chem. Phys.* **1997**, *215*, 167.
(9) Szichman, H.; Varandas, A. J. C.; Baer, M. *Chem. Phys. Lett.* **1994**, *231*, 253.
(10) Szichman, H.; Varandas, A. J. C.; Baer, M. *J. Chem. Phys.* **1995**, *102*, 3474.
(11) Balakrishnan, N.; Billing, G. D. *J. Chem. Phys.* **1996**, *104*, 9482.
(12) Varandas, A. J. C.; Llanio-Trujillo, J. L. *J. Theor. Comput. Chem.* **2002**, *1*, 31.
(13) Varandas, A. J. C. *Int. Rev. Phys. Chem.* **2000**, *19*, 199.
(14) Roos, B. O.; Andersson, K.; Fülsher, M. P.; Malmquist, P.-A.; Serrano-Andrés, L.; Pierloot, K.; Merchán, M. *Adv. Chem. Phys.* **1996**, *93*, 219.
(15) Hernández-Lamoneda, R.; Hernández, M. I.; Campos-Martínez, J. *Chem. Phys. Lett.* **2003**, *368*, 709.
(16) Hernández-Lamoneda, R.; Ramírez-Solis, A. *Chem. Phys. Lett.* **2000**, *321*, 191.
(17) Hernández-Lamoneda, R.; Ramírez-Solis, A. *J. Chem. Phys.* **2000**, *113*, 4139.
(18) Varandas, A. J. C.; Llanio-Trujillo, J. L. *Chem. Phys. Lett.* **2002**, *356*, 585.
(19) Varandas, A. J. C. *Adv. Chem. Phys.* **1988**, *74*, 255.
(20) Varandas, A. J. C. *Lecture Notes in Chemistry*; Laganá, A., Riganelli, A., Eds.; Springer: Berlin, Germany, 2000; Vol. 75, p 33.
(21) Varandas, A. J. C. *Conical Intersections*: *Electronic Structure, Dynamics and Spectroscopy*; Yarkony, D., Köppel, H., Domcke, W., Eds.; World Scientific Publishing: Singapore (in press).
(22) Atkinson, R.; Baulch, D. L.; Cox, R. A.; Hampson, R. F., Jr.; Kerr, J. A.; Troe, J. *J. Phys. Chem. Ref. Data* **1992**, *21*, 1125.
(23) Xantheas, S. S.; Atchity, G. J.; Elbert, S. T.; Ruedenberg, K. *J. Chem. Phys.* **1991**, *94*, 8054.
(24) Varandas, A. J. C. *J. Phys. Chem. A* **2003**, *107*, 3769.
(25) Mayne, H. R. *Dynamics of Molecules and Chemical Reactions*; Wyatt, R., Zhang, J., Eds.; Marcel Dekker: New York, 1996; p 589.
(26) Peslherbe, G. H.; Wang, H.; Hase, W. L. *Adv. Chem. Phys.* **1999**, *105*, 171.
(27) Krishnan, R.; Binkley, J. S.; Pople, J. A. *J. Chem. Phys.* **1980**, *72*, 650.
(28) Lauvergnat, D.; Clary, D. *J. Chem. Phys.* **1998**, *108*, 3566.
(29) Hase, W. L. MERCURY: a general Monte Carlo classical trajectory computer program, QCPE no. 453. An updated version of this code is VENUS96: Hase, W. L.; Duchovic, R. J.; Hu, X.; Komornik, A.; Lim, K. F.; Lu, D.-H.; Peslherbe, G. H.; Swamy, K. N.; van de Linde, S. R.; Varandas, A. J. C.; Wang, H.; Wolf, R. J. *QCPE Bull.* **1996**, *16*, 43.
(30) Varandas, A. J. C.; Pais, A. A. C. C.; Marques, J. M. C.; Wang, W. *Chem. Phys. Lett.* **1996**, *249*, 264.
(31) Varandas, A. J. C.; Brandão, J.; Pastrana, M. R. *J. Chem. Phys.* **1992**, *96*, 5137.
(32) Jongma, R. T.; Wodtke, A. M. *J. Chem. Phys.* **1999**, *111*, 10957.
(33) Balakrishnan, N.; Dalgarno, A.; Billing, G. D. *Chem. Phys. Lett.* **1998**, *288*, 657.
(34) Steinfeld, J. I.; Francisco, J. S.; Hase, W. L. *Chemical Kinetics and Dynamics*; Prentice-Hall: Englewood Cliffs, NJ, 1989.
(35) Coletti, C.; Billing, G. D. *Chem. Phys. Lett.* **2002**, *356*, 14.
(36) Miller, R. L.; Suits, A. G.; Houston, P. L.; Toumi, R.; Mack, J. A.; Wodtke, A. M. *Science* **1994**, *265*, 1831.
(37) Varandas, A. J. C. *ChemPhysChem* **2002**, *3*, 433.